First NNLO fragmentation functions of K_S^0 and $\Lambda/\bar{\Lambda}$ and their uncertainties in the presence of hadron mass corrections

Maryam Soleymaninia[⦿],[1,*] Hamed Abdolmaleki[⦿],[1,†] and Hamzeh Khanpour[⦿][2,1,‡]

[1]*School of Particles and Accelerators, Institute for Research in Fundamental Sciences (IPM),*
P.O.Box 19395-5531, Tehran, Iran
[2]*Department of Physics, University of Science and Technology of Mazandaran,*
P.O.Box 48518-78195, Behshahr, Iran

The current paper presents a determination of K_S^0 and $\Lambda/\bar{\Lambda}$ fragmentation functions (FFs) from QCD analysis of single-inclusive electron-positron annihilation process (SIA). Our FFs determinations are performed at next-to-leading order (NLO), and for the first time, at next-to-next-to-leading order (NNLO) accuracy in perturbative quantum chromodynamics (pQCD) which is designated as SAK20 FFs. Each of these FFs is accompanied by their uncertainties which are determined using the "Hessian" method. Considering the hadron mass corrections, we clearly investigate the reliability of our results upon the inclusion of higher-order QCD correction. We provide comparisons of SAK20 FFs set with the available analysis from another group, finding in general a reasonable agreement, and also considerable differences. In order to judge the fit quality, our theoretical predictions are compared with the analyzed SIA datasets. SAK20 FFs at NLO and NNLO accuracy along with their uncertainties are made available in the standard LHAPDF format in order to use for predictions of present and future measurements in high-energy collisions such as LHC and RHIC.

I. INTRODUCTION

In perturbative quantum chromodynamics (pQCD), unpolarized fragmentation functions (FFs) are necessary ingredients to calculate the cross section of inclusive single hadron production in hard scattering processes [1–12]. In perturbative QCD, Collinear FFs $D_i^h(z, \mu_F^2)$ can be expressed as a probability for a parton i at the factorization scale μ_F to fragment into a hadron h which carries the fraction z of the parton momentum.

In addition to study the z dependence of FFs, we can study the FFs dependency on transverse momentum, P_{hT} which are called the transverse momentum dependent fragmentation functions (TMD FFs) [13–17]. From the factorization theorem [18], the leading twist term of single hadron inclusive production measurements can be interpreted as the convolution of universal FFs with partonic cross sections of real partons, to account for any hadrons in the final state.

The main motivation to improve our understanding of the details of the subsequent hadronization process is provided by the fact that the FFs along with their associated uncertainties play an important role in several applications in hard scattering processes for the present or future hadron colliders such as LHC, LHeC and RHIC [19–24].

To begin with, FFs represent one of the dominant theoretical uncertainties at the LHC measurements. FFs along with their uncertainties also affect the productions of light and heavy hadrons at LHC [25,26]. A second example is the precise measurement of SM parameters at hadron colliders such as LHC, and future high-energy LHC (HE-LHC) and proposed post-LHC particle accelerator in which called Future Circular Collider (FCC) [27–29].

Several collaborations provide regular updates of their light and heavy hadrons FFs sets with uncertainties, see for example [1,3–6,12,30] and references therein. For the K_S^0 and $\Lambda/\bar{\Lambda}$ FFs which are the main aim of this paper, the results by BKK96 [31], BS [32], AKK05 [33] and AKK08 [34] Collaborations are available in the literature. In Ref. [31], the authors presented new sets of FFs for neutral kaons both at leading order (LO) and NLO accuracy. The inclusive K^0 production in electron-positron annihilation taken by Mark II at SLAC PEP and by ALEPH at CERN LEP have been used. BS Collaboration [32] has calculated

*Maryam_Soleymaninia@ipm.ir
†Abdolmaleki@ipm.ir
‡Hamzeh.Khanpour@cern.ch

unpolarized FFs for the octet baryons by including some data on proton and Λ production in unpolarized DIS [35,36] in addition to octet baryons production in e^+e^- annihilation. In addition, AKK05 [33] obtained FFs for K_S^0 and Λ at NLO accuracy by a QCD analysis using the data from electron-positron collisions. In order to separate the light quark flavor FFs, they have also included for the first time the quark tagging probabilities from OPAL Collaboration [37]. Finally, AKK08 [34] updated their previous study on K_S^0 and Λ FFs, AKK05 [33], and also pion, kaon and proton FFs have been determined in this paper, by adding the inclusive hadron production measurements from proton-proton collisions at PHENIX, STAR, BRAHMS and CDF to their data sample of SIA. They also considered the hadron mass effects in their QCD analyses. Actually the last QCD analysis for fragmentation functions of K_S^0 and Λ have been done by AKK08.

There is a range of differences between the K_S^0 and $\Lambda/\bar{\Lambda}$ FFs determined in the mentioned studies and the QCD analyses done in this paper, arising for example at the level of the selection of the input fitted experimental data, methodological choices for the parametrization of FFs, the detailed estimate, and propagation of the FFs uncertainties and finally the presence of high order perturbative QCD corrections.

The FFs presented in this study introduce some methodological and theoretical improvements over previous determinations available in the literature. The main aim of this paper is to extract the FFs of K_S^0 and $\Lambda/\bar{\Lambda}$ along with their uncertainties from a QCD analysis of single-inclusive electron-positron annihilation process (SIA). It should be noted here that the FFs uncertainties for K_S^0 and $\Lambda/\bar{\Lambda}$ are calculated for the first time in this paper. In addition, this analysis has been done for the first time, at next-to-next-to-leading (NNLO) accuracy in perturbative QCD. The other determinations of K_S^0 and $\Lambda/\bar{\Lambda}$ FFs in the literature are restricted to the NLO accuracy in perturbative QCD without determination of their uncertainties. However, the estimation of the FFs uncertainty for the results presented in Ref. [34] has been worked out in a review article by S. Albino in Ref. [38].

In order to achieve a reliable estimate of the uncertainties of K_S^0 and $\Lambda/\bar{\Lambda}$ FFs, we use the Hessian approach developed in Refs. [39,40]. We discuss the fit quality, the perturbative convergence upon inclusion of higher-order QCD corrections, and the effect arising from the hadron mass corrections. Finally, we compare our FFs determined in this study to other recent sets of FFs available in the literature. Although, in general, we find reasonable agreements, some important differences are also seen. The effect arising from the hadron-mass corrections on the FFs are carefully investigated and discussed in the text.

The following paper is organized as follows: In Sec. II, we discuss in detail the SIA experimental data along with

their corresponding observables and the kinematic cuts which are imposed to determine the FFs for K_S^0 and $\Lambda/\bar{\Lambda}$. In Sec. III, we present the theoretical details of the SAK20 determination for K_S^0 and $\Lambda/\bar{\Lambda}$ FFs including the evolution of FFs and the hadron mass corrections. SAK20 parametrizations and our assumptions are discussed in detailed in Sec. IV. Then, Sec. V deals with the χ^2 minimization and the method for calculation of FFs uncertainty. The main results and findings that emerged from this study are presented and discussed in detail in Sec. VI. We first turn to discuss the SAK20 FFs sets for the K_S^0 and $\Lambda/\bar{\Lambda}$. Then, we compare our FFs set NLO and NNLO with other results in the literature. In Sec. VII we also present comparisons between all analyzed SIA data and the corresponding theoretical predictions obtained using the SAK20 FFs. Finally in Sec. VIII, we study the impact of hadron mass corrections at NNLO accuracy for both K_S^0 and $\Lambda/\bar{\Lambda}$ FFs. Section IX presents our summary and conclusions.

II. EXPERIMENTAL OBSERVABLES

In this section we discuss in details the experimental data used for determination of K_S^0 and $\Lambda/\bar{\Lambda}$ FFs. First, we present the datasets from different experiments and their references. Then, the kinematical cuts applied to the datasets at small range of z will be explained. Finally, we report the χ^2 for all experimental collaborations individually both at NLO and NNLO accuracy.

In our analysis, the data included to extract FFs for K_S^0 and $\Lambda/\bar{\Lambda}$ are correspond to the inclusive e^+e^- annihilation and single hadron production which cover the several range of center-of-mass energies. The K_S^0 production datasets included in SAK20 analysis is summarized in Table I. We specify the name of the experiments, the corresponding references, the measured observables, and the number of data points included in the fit. The values of the χ^2 per data point for both the individual and the total datasets are also reported in this table at NLO and NNLO accuracy. To obtain FFs for $q + \bar{q} \rightarrow K_S^0$, we use the untagged data from TASSO collaboration at $\sqrt{s} = 14$, 22 and 34 GeV [41] and at $\sqrt{s} = 14.8$, 21.5, 34.5, 35 and 42.6 GeV [42]. Our datasets also include the data from HRS [43], TPC [44], and MARK II [45] Collaborations at $\sqrt{s} = 29$ GeV. The data from CELLO Collaboration at $\sqrt{s} = 35$ GeV [46] and TOPAZ Collaboration at $\sqrt{s} = 58$ GeV [47] also considered. The datasets used in our analysis also include the untagged data at $\sqrt{s} = M_Z$ which are measured by ALEPH [48], DELPHI [49], OPAL [37], and SLD [50] Collaborations. In addition, the measurements from DELPHI Collaboration at $\sqrt{s} = 183$ and 189 GeV [51] are included in our datasets. Finally, in order to determine the well-constrained light and heavy quarks FFs, the (u, d, s)-, c- and b-tagged data from SLD collaboration at $\sqrt{s} = M_Z$ are also added to our data sample.

TABLE I. The list of input datasets included in analyses of K_S^0 FFs at NLO and NNLO accuracy. For each dataset, we indicate the corresponding published reference, the name of the experiments, the measured observables, the center-of-mass energy $\sqrt{s}$ and the value of χ^2 per data point for the individual dataset at NLO and NNLO accuracy. The total values of χ^2/d.o.f. have been presented as well.

Experiment	Data type	$\sqrt{s}$	# data	χ^2_{NLO} (K_S^0)	χ^2_{NNLO} (K_S^0)
TASSO[41]	Inclusive	14	9	9.804	9.128
TASSO [42]	Inclusive	14.8	9	16.307	15.440
TASSO [42]	Inclusive	21.5	6	2.736	2.756
TASSO [41]	Inclusive	22	6	4.979	5.111
HRS [43]	Inclusive	29	11	22.444	23.433
TPC [44]	Inclusive	29	8	4.559	4.091
MARKII [45]	Inclusive	29	18	7.979	7.222
TASSO [41]	Inclusive	34	14	21.667	22.131
TASSO [42]	Inclusive	34.5	14	17.353	17.395
TASSO [42]	Inclusive	35	14	21.226	19.314
CELLO [46]	Inclusive	35	9	3.915	3.417
TASSO [42]	Inclusive	42.6	14	9.386	10.070
TOPAZ [47]	Inclusive	58	4	2.994	2.806
ALEPH [48]	Inclusive	91.2	16	17.630	12.731
DELPHI [49]	Inclusive	91.2	13	7.450	7.695
OPAL [37]	Inclusive	91.2	16	9.139	8.494
SLD [50]	Inclusive	91.2	9	5.398	4.795
SLD [50]	uds tag	91.2	9	8.135	8.093
SLD [50]	c tag	91.2	9	11.108	11.731
SLD [50]	b tag	91.2	9	10.470	10.735
DELPHI [51]	Inclusive	183	3	8.103	8.325
DELPHI [51]	Inclusive	189	4	8.481	8.436
Total χ^2/d.o.f.			224	1.161	1.124

TABLE II. Same as in Table I, but for $\Lambda/\bar{\Lambda}$.

Experiment	Data type	$\sqrt{s}$	# data	χ^2_{NLO} ($\Lambda/\bar{\Lambda}$)	χ^2_{NNLO} ($\Lambda/\bar{\Lambda}$)
TASSO [41]	Inclusive	14	3	0.509	0.501
TASSO [41]	Inclusive	22	4	2.105	2.197
HRS [43]	Inclusive	29	12	9.507	9.261
MARKII [45]	Inclusive	29	15	9.978	9.930
TASSO [41]	Inclusive	33.3	5	7.611	7.516
TASSO [42]	Inclusive	34	7	7.564	7.286
TASSO [42]	Inclusive	34.8	10	33.276	34.355
CELLO [46]	Inclusive	35	7	4.196	3.981
TASSO [42]	Inclusive	42.1	5	7.472	7.575
ALEPH [48]	Inclusive	91.2	17	30.509	31.038
DELPHI [49]	Inclusive	91.2	8	21.243	20.904
OPAL [37]	Inclusive	91.2	13	11.821	12.229
SLD [50]	Inclusive	91.2	10	18.521	18.324
SLD [50]	uds tag	91.2	5	7.464	7.260
SLD [50]	c tag	91.2	5	5.286	5.100
SLD [50]	b tag	91.2	5	1.363	1.437
DELPHI [51]	Inclusive	183	3	4.238	4.112
DELPHI [51]	Inclusive	189	3	4.575	4.395
Total χ^2/d.o.f.			137	1.601	1.602

and in Fig. 2 for the $\Lambda/\bar{\Lambda}$ production in SIA processes. The applied kinematic cut $z < 0.05$ is illustrated by the vertical dotted lines in the plots. The range of Q for both hadrons varies from the low energy TASSO data with $Q = 14$ GeV to the high energy $Q = 189$ GeV from DELPHI Collaboration. As can be seen, a large number of data points are available for the small z region ($z < 0.6$).

Our baseline determinations of K_S^0 and $\Lambda/\bar{\Lambda}$ FFs are based on the data points described above. Since toward the small z region, soft gluon effects lead the DGLAP evolution equation becomes unstable, then the models fall down the experimental data. Hence, all the theoretical models restrict their analyses to the data points with $z \geq z_{\min}$ in which $z_{\min}$ indicates to the low-z cut. The QCD analyses for K_S^0 and $\Lambda/\bar{\Lambda}$ in Refs. [31–33] excluded the low z regions with $z < 0.1$ and the hadron mass corrections were not considered in their studies. We should stress here that the recent studies have shown that the mass corrections have an important key role in the small z region. Like for the analysis by AKK08 [34], we consider the hadron mass corrections to be able to include more low-z data points by imposing a kinematic cut at the small values of z; $z_{\min} = 0.05$. Hence, we restrict our data sample to the data points with $z \geq z_{\min} = 0.05$ for both K_S^0 and $\Lambda/\bar{\Lambda}$ analyses. The number of data points after the mentioned kinematical cut for our K_S^0 and $\Lambda/\bar{\Lambda}$ analyses are 224 and 137, respectively.

III. THE QCD FRAMEWORK AND HADRON MASS CORRECTIONS

QCD formalism allows us to express the hard scattering cross section in the term of a convolution of the perturbative

Likewise, in order to calculate the FFs for $q + \bar{q} \to \Lambda/\bar{\Lambda}$, all available SIA datasets are included. The analyzed untagged data include the data from TASSO Collaboration at $\sqrt{s} = 14$, 22 and 33.3 GeV [41], the HRS [43] and MARK II [45] Collaborations at $\sqrt{s} = 29$ GeV, the TASSO Collaboration at $\sqrt{s} = 34$, 34.8 and 42.1 GeV [42]. The datasets also include the data from CELLO Collaboration at $\sqrt{s} = 35$ GeV [46]. We also use the ALEPH [48], DELPHI [49], OPAL [37], and SLD [50] Collaborations at $\sqrt{s} = M_Z$. In addition, the data from DELPHI Collaboration at $\sqrt{s} = 183$ and 189 GeV [51] also included in our data sample. Finally, in order to separate the individual quark flavors, we use the (u, d, s)-, c- and b-tagged data from SLD Collaboration at $\sqrt{s} = M_Z$ [50]. The datasets analyzed in our $\Lambda/\bar{\Lambda}$ QCD fit are listed in Table II. In this table, the experimental Collaborations and the corresponding published reference, the observable and the center-of-mass energies are listed. The table also include the values of the χ^2 per data point in the individual and total datasets extracted at both NLO and NNLO accuracy.

All the experimental data which we used in this analysis in the (z, Q) plane are shown in Fig. 1 for the K_S^0 production

FIG. 1.   Kinematic reach of experimental SIA data in the (z, Q) plane used to determine the K_S^0 FFs.

partonic cross sections and nonperturbative distribution functions. The scale dependence of nonperturbative FFs can be obtained by the timelike DGLAP evolution equation in z-space. The computation of the cross section for the SIA processes along with the DGLAP evolution equations is publicly available up to NNLO accuracy via the APFEL package [52].

The cross section for the single inclusive electron-positron annihilation in production of strange particles K_S^0 and $\Lambda/\bar{\Lambda}$, $e^+e^- \to h(K_S^0; \Lambda/\bar{\Lambda}) + X$, can be given in terms of timelike structure functions, $F_T(z, Q^2)$ and $F_L(z, Q^2)$ which can be

written in terms of convolutions of nonperturbative unpolarized FFs D_i^h and perturbative partonic cross sections C_i. Hence, the differential cross section is given by,

$$\frac{1}{\sigma_{tot}} \frac{d\sigma^h}{dz} = F_T^h + F_L^h$$

$$= \frac{1}{\sigma_{tot}} \sum_i \int_z^1 \frac{dx}{x} C_i\left(x, \alpha_s(\mu), \frac{Q^2}{\mu^2}\right) D_i^h\left(\frac{z}{x}, \mu^2\right),$$

$$(1)$$
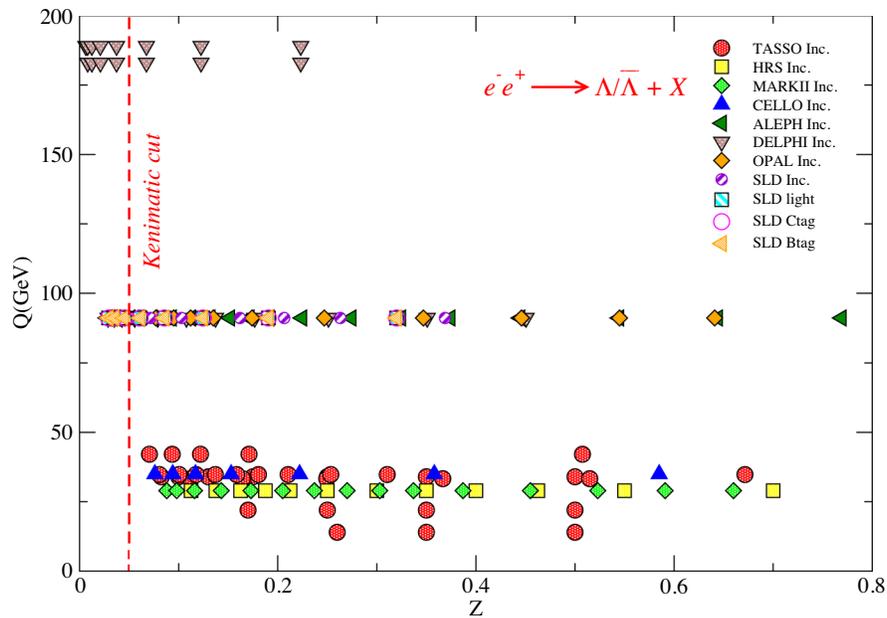
FIG. 2.   Same as Fig. 1 but for the $\Lambda/\bar{\Lambda}$ data.

where the SIA differential cross section was normalized to the total cross section σ_{tot} as,

$$\sigma_{\text{tot}}(Q) = \frac{4\pi\alpha^2(Q)}{Q^2} \sum_q^{n_f} \hat{e}_q^2(Q)(1 + \alpha_s K_{\text{QCD}}^{(1)} + \alpha_s^2 K_{\text{QCD}}^{(2)} + \cdots).$$

(2)

Here $K_{\text{QCD}}^{(i)}$ show the QCD corrections and have been known yet up to $\mathcal{O}(\alpha_s^3)$. The scaling variable is defined as $z = 2P_h.q/q^2$ with hadron four-momentum P_h and γ/Z four momentum q. For the structure functions $F_T(z, Q^2)$ and $F_L(z, Q^2)$ presented in Eq. (1), the Wilson coefficient C_i functions can be written as expansions in term of strong coupling constant. It reads,

$$C_{ji}\left(z, \alpha_s(\mu), \frac{Q^2}{\mu^2}\right) = (1 - \delta_{jL})\delta_{iq}\delta(1 - z)$$

$$+ \frac{\alpha_s(\mu)}{2\pi} c_{ji}^{(1)}\left(z, \frac{Q^2}{\mu^2}\right)$$

$$+ \left(\frac{\alpha_s(\mu)}{2\pi}\right)^2 c_{ji}^{(2)}\left(z, \frac{Q^2}{\mu^2}\right) + \cdots, \quad (3)$$

where $j = $ T, L. These coefficient functions are calculated up to the NNLO accuracy in Refs. [53–55]. Note that the nonperturbative universal function, $D_i^h(z, \mu^2)$ describes density for fragmenting unpolarized parton i into the unpolarized hadron h which carry fraction z of the longitudinal momentum of the incoming parton. In order to calculate the parton FFs at the different scales of energy $\mu^2 > \mu_o^2$, the perturbative QCD corrections lead to use the time-like DGLAP evolution equations [56–59] which is given by,

$$\frac{\partial D_i^h(z, \mu^2)}{\partial \ln \mu^2} = \sum_j \int_z^1 \frac{dx}{x} P_{ji}(x, \alpha_s(\mu^2)) D_j^h\left(\frac{z}{x}, \mu^2\right), \quad (4)$$

where $P_{ji}(x, \alpha_s(\mu^2))$ are the timelike splitting functions and describe splitting process $i \rightarrow j + X$. These functions can be written as perturbative expansions in term of strong coupling constant which have been calculated up to NNLO accuracy in Refs. [60,61].

Hadron mass effects and the heavy quark mass corrections are considered in connection with charmed meson production in Ref. [62] in zero-mass (ZM) and general-mass (GM) variable flavor number schemes, respectively. In the calculation of the partonic cross section of heavy quark production through the initial conditions of the SIA process, the non-zero values of heavy quark masses should be considered. However, the mass of heavy hadrons changes the lower bound on the scaling variable z, $4m_h^2/s \leq z \leq 1$. Consequently, the effects of hadron and the quark mass corrections could improve the description of experimental data. The authors in Ref. [62] have mentioned

that the hadron mass effects are more important than the quark mass, and hence, the prior one is essential to describe the measured cross sections at low values of z.

In the AKK08 [34] analysis the hadron mass effects are studied for $\pi^\pm$, $K^\pm$, $p/\bar{p}$, K_S^0 and $\Lambda/\bar{\Lambda}$. In their analysis the hadron masses considered as independent parameters in fit procedure. In addition, the hadron mass effects have been investigated in Refs. [5,63] for charmed meson and proton productions in SIA processes. We follow the strategy presented in Refs. [5,63] to consider such corrections in our analyses.

In the presence of hadron mass effects with the parameter m_h as a hadron mass, the scaling variable need to be modified from $z = 2E_h/\sqrt{s}$ to a specific choice of scaling variable η defined as a light-cone scaling. It is given by,

$$\eta = \frac{z}{2}\left(1 + \sqrt{1 - \frac{4m_h^2}{sz^2}}\right).$$

(5)

Consequently, the differential cross section in the presence of hadron mass effects for a SIA process need to be modified as

$$\frac{d\sigma}{dz} = \frac{1}{1 - \frac{m_h^2}{s\eta^2}} \sum_a \int_\eta^1 \frac{dx_a}{x_a} \frac{d\hat{\sigma}_a}{dx_a} D_a^h\left(\frac{\eta}{x_a}, \mu\right).$$

(6)

The values of the hadron masses used in Eqs. (5) and (6) are considered to be $m_{K_S^0} = 0.4976$ and $m_\Lambda = 1.115$ GeV [64]. The above equation for the differential cross section is applied in our K_S^0 and $\Lambda/\bar{\Lambda}$ analyses to consider the hadron mass effects. Equation (6) indicates that including the hadron mass corrections and the effects arising from that, strongly depend on the hadron mass m_h, and hence, the kind of hadron.

We should mentioned here that, for the numerical calculations of the timelike DGLAP equations we use the modified minimal-subtraction ($\overline{\text{MS}}$) factorization scheme. We also used the zero-mass variable-flavor-number scheme (ZM-VFNS) which is implemented at open source framework, APFEL [52]. This scheme assumes that quark mass is set to zero. We applied some modifications in APFEL to take into account the hadron mass corrections. We choose the heavy flavor masses $m_c = 1.51$ GeV and $m_b = 4.92$ GeV, and we take $\mu_r = \mu_f = Q$ for the QCD renormalization and factorization scales. In our analyses, the QCD running coupling constant is fixed to $\alpha_s(M_Z) = 0.118$ [64]. This selection for the strong coupling constant is consistent with very recent determination of the $\alpha_s(M_Z)$ reported by the NNPDF3.1 Collaboration [65].

As a short summary, in this section, was briefly review the pQCD framework for the electron-positron annihilation process, the QCD factorization, and the timelike evolution equation up to NNLO accuracy. We refer the reader to the

Refs. [1,34] for more details on the QCD framework. Since our aim in this analysis is to investigate the effect of higher order perturbative corrections, we will clearly discuss in Sec. VI the improvements to the fit quality, the value of χ^2 for each dataset, and the total $\chi^2/\text{d.o.f.}$ at NLO and NNLO accuracy. The comparison of the central values and error bands of K_S^0 and $\Lambda/\bar{\Lambda}$ FFs in these two perturbative orders will be presented in Sec. VI as well.

IV. THE TECHNICAL FRAMEWORK AND OUR PARAMETRIZATION

In the following section, we are in a position to describe our methodology, the input parametrization, and the assumptions that we consider to extract the K_s^0 and $\Lambda/\bar{\Lambda}$ FFs from perturbative QCD analysis to the available SIA experimental data.

Since the main goal in this analysis is to investigation of the FFs of K_s^0 and $\Lambda/\bar{\Lambda}$, we should parametrized the light and heavy quark FFs at initial scale $Q_0 = 5$ GeV which should be above the bottom mass threshold in ZM-VFNS. Then QCD evolution will help us to achieve it at arbitrary scale Q. In this analysis we use the most flexible parametrization form for the K_S^0 and $\Lambda/\bar{\Lambda}$ FFs with $n_f = 5$ active flavor in which widely used in the analysis of different hadrons in the literature [9,34,66]. Most recently, we also considered such parametrization for the determination of unidentified light charged hadron and pion FFs analyses [4,67]. This parametrization is given by,

$$D_i^{h^\pm}(z, Q_0) = \mathcal{A}_i \mathcal{N}_i z^{\alpha_i}(1-z)^{\beta_i}[1 + \gamma_i(1-z)^{\delta_i}], \quad (7)$$

where the free parameters are $\mathcal{N}_i$, α_i, β_i, γ_i, and δ_i and $\mathcal{A}_i$ is the normalization factor. In the above parametrization form $\mathcal{N}_i$ and $\mathcal{A}_i$ are not independent, $\mathcal{N}_i$ is the second moment of the parton fragmentation function and $\mathcal{A}_i$ is the normalization factor which can be computed to be:

$$\frac{1}{\mathcal{A}_i} = B[2 + \alpha_i, \beta_i + 1] + \gamma_i B[2 + \alpha_i, \beta_i + \delta_i + 1]. \quad (8)$$

where $B[a, b]$ is the Euler Beta function. Note that by including only the SIA data in the QCD fit, it is not possible to separate the quark and anti-quark FFs, then we use the quark combination $q^+ = q + \bar{q}$ in the parametrization form. In Eq. (7), i indicates to the d^+, u^+, s^+, c^+, b^+, and g.

Now we are in a position to discuss our assumptions for the parametrization of K_S^0 FFs. Considering the quark content of the $K_S^0(d\bar{s})$, we assume asymmetry between light quarks u, d, s, and parametrize them separately as like heavy quarks and gluon. Since statistically the number of experimental data points from e^+e^- annihilation to determine the K_S^0 is rather limited, all the parameters cannot be well constrained by these datasets. The parameters γ and δ are free for d^+, b^+, and g and they need to determine from

TABLE III. Best-fit parameters for the fragmentation of partons into K_S^0 at NLO and NNLO accuracy with a framework introduced in Sec. III. The starting scale has been taken to be $Q_0 = 5$ GeV for all parton species.

Parameter	NLO	NNLO
$\mathcal{N}_{u^+}$	0.007	0.006
α_{u^+}	12.911	12.574
β_{u^+}	155.570	155.383
$\mathcal{N}_{d^+}$	0.443	0.448
α_{d^+}	−1.885	−1.884
β_{d^+}	0.948	0.937
γ_{d^+}	−0.999	−0.999
δ_{d^+}	0.001	0.001
$\mathcal{N}_{s^+}$	0.118	0.119
α_{s^+}	1.302	1.297
β_{s^+}	8.507	8.553
$\mathcal{N}_{c^+}$	0.171	0.169
α_{c^+}	−0.038	−0.112
β_{c^+}	4.011	4.008
$\mathcal{N}_{b^+}$	0.085	0.085
α_{b^+}	0.696	0.740
β_{b^+}	19.858	19.506
γ_{b^+}	−1.339	−1.830
δ_{b^+}	−2.043	−2.268
$\mathcal{N}_g$	0.016	0.017
α_g	1.203	1.227
β_g	5.228	6.216
γ_g	70.074	99.014
δ_g	76.396	81.148

the QCD fit. For the rest, we fix γ_{u^+,s^+,c^+} and δ_{u^+,s^+,c^+} to zero. Consequently, the remaining 24 free independent fit parameters of FFs are determined by a standard χ^2 minimization method. Best-fit parameters for the fragmentation of partons into K_S^0 obtained through our NLO and NNLO analyses are listed in Table III.

The $\Lambda/\bar{\Lambda}$ baryon contains the (uds) quarks. Hence, we define separate parametrization for all light quarks and we do not assume SU(2) or SU(3) symmetry for $\Lambda/\bar{\Lambda}$. Since the number of available data for the $\Lambda/\bar{\Lambda}$ production in SIA process is not enough to constrain all independent fit parameters in Eq. (7), we prefer to consider a simple form of parametrization and fix $\gamma = 0$ and $\delta = 0$ for all flavors except for the gluon density. The total number of free parameters for Λ FFs is 20. The best-fit parameters for the quarks and gluon FFs of $\Lambda/\bar{\Lambda}$ at NLO and NNLO accuracy are presented in Table IV.

V. χ^2 MINIMIZATION AND METHOD OF ERROR CALCULATION

Our fitting methodology and χ^2 minimization and the uncertainty estimation have been described at length in our

TABLE IV. Same as in Table III, but for $\Lambda/\bar{\Lambda}$ FFs.

Parameter	NLO	NNLO
$\mathcal{N}_{u^+}$	0.033	0.032
α_{u^+}	3.788	3.215
β_{u^+}	13.409	12.050
$\mathcal{N}_{d^+}$	0.101	0.114
α_{d^+}	−1.043	−1.179
β_{d^+}	3.140	2.379
$\mathcal{N}_{s^+}$	0.008	0.006
α_{s^+}	83.249	82.584
β_{s^+}	85.373	86.038
$\mathcal{N}_{c^+}$	0.026	0.028
α_{c^+}	0.967	0.708
β_{c^+}	20.293	18.191
$\mathcal{N}_{b^+}$	0.048	0.047
α_{b^+}	−0.762	−0.713
β_{b^+}	3.331	3.845
$\mathcal{N}_g$	0.015	0.013
α_g	6.704	17.189
β_g	2.029	8.613
γ_g	−0.299	−0.751
δ_g	−0.187	0.193

previous publications [4–6] on the same subjects. In this section, we briefly review methodology specific to the K_S^0 and $\Lambda/\bar{\Lambda}$ FFs determinations. We first discuss the minimization strategy to optimize the independent fit parameters, and then we present the uncertainty estimations.

As we mentioned earlier, we perform our QCD analysis using the standard functional form at the initial scale of μ_0, then we evolve the FFs from the initial scale up to arbitrary scale using the DGLAP evolution equation [56–59] to calculate the physical observable. By comparing the theoretical prediction with the corresponding experimental data in the full kinematic range, we determine the unknown FF parameters by constructing a global χ^2 function using the experimental measurement and theoretical prediction for ith data point. The χ^2 function is minimized using the CERN MINUIT package [68] and is constructed as follows:

$$\chi^2_{\text{global}} = \sum_{i=1}^{n^{\text{Exp}}} w_i \chi^2_i$$

$$= \sum_{i=1}^{n^{\text{Exp}}} w_i \left[\frac{(\mathcal{K}_i - 1)^2}{(\Delta\mathcal{K}_i)^2} + \sum_{j=1}^{n^{\text{Data}}} \left(\frac{\mathcal{K}_i \mathcal{O}_{1,j}^{\text{Exp}} - F_{1,j}^{\text{Theory}}}{\mathcal{K}_i \Delta\mathcal{O}_{1,j}^{\text{Exp}}} \right)^2 \right],$$

(9)

where the weight factor w_i allows us to apply separate weights to different experimental datasets which in this analysis we take it to be unity. The index i sums over all experimental datasets. For each dataset, the index j sums

over all data points. $F_{1,j}^{\text{Theory}}$ is the theoretical prediction for jth bin, $\Delta\mathcal{O}_{1,j}^{\text{Exp}}$ is included the statistical and systematic errors which we combine in quadrature, and $\mathcal{O}_{1,j}^{\text{Exp}}$ is the measured value of the ith data point. In the above, the normalization shifts $\mathcal{K}_i$ for each experiment, are fitted at the first step of our procedure, and then keep fixed in our analysis. Note that the associated normalized uncertainty $\Delta\mathcal{K}_i$ is obtained by experimental setup.

We now describe the methodology that we applied in this study for the estimation of the K_S^0 and $\Lambda/\bar{\Lambda}$ FFs uncertainties. Large amount of QCD analyses use the 'Hessian' method to calculate the FFs uncertainties which is based on tolerance parameter T. They consider $\Delta\chi^2 = T^2$ which ensures that each dataset is described within the desired confidence level (CL). The standard error propagation which is given by the statistical error on any given quantity q, is defined as:

$$(\sigma_q)^2 = \Delta\chi^2 \left(\sum_{\alpha,\beta} \frac{\partial q}{\partial p_\alpha} C_{\alpha,\beta} \frac{\partial q}{\partial p_\beta} \right).$$

(10)

To calculate the fully 1-σ error bands for the FFs, one could use the Hessian matrix definition, $H_{\alpha,\beta} = \frac{1}{2}\partial^2\chi^2/\partial p_\alpha \partial p_\beta$ which is inverse of the covariance matrix $C = H^{-1}$ that is obtained at the χ^2 minimum. In this analysis, we adopt the standard parameter fitting criterion by choosing the $T = 1$, which corresponds to the 68% CL, i.e., 1-σ error bands. The details of the "Hessian method" are fully addressed in Refs. [39,40], and we refer the reader to these published works for more details.

VI. THE RESULTS OF FFs ANALYSIS

The following part of this paper describes in greater details the results of SAK20 K_S^0 and $\Lambda/\bar{\Lambda}$ FFs with their uncertainties. First, we present the best-fit parameters for the fragmentation of partons to K_S^0 and $\Lambda/\bar{\Lambda}$. Second, we present SAK20 FFs at NLO and NNLO accuracy and compare them with each other. Next, we quantify the perturbative convergence of the SAK20 FFs upon the inclusion of higher-order QCD corrections. Finally, we compare SAK20 FFs with the corresponding results by AKK08 FFs Collaboration [34]. We show that there are conspicuous differences between SAK20 and AKK08 FFs, specially for light quarks and gluon. As we mentioned before, we will divided our analysis into two separate fit. The first one is perform a fit with all data of Table I to extract the K_S^0 partonic FFs using the K_S^0 meson production in SIA process, and we identify this as SAK20 K_S^0 FF, and the second one is perform a fit with all data of Table II to extract the $\Lambda/\bar{\Lambda}$ partonic FFs using the $\Lambda/\bar{\Lambda}$ baryon production in SIA process, and we identify this as SAK20 $\Lambda/\bar{\Lambda}$ FFs. In the following, we will present the resulting

FFs along with their uncertainties. We present the results of K_S^0 FFs and their uncertainties in Sec. VI A, and in Sec. VI B, the results of $\Lambda/\bar{\Lambda}$ FFs along with their error bands will be discussed in details.

A. The results of K_S^0 FFs and their uncertainties

To initiate the discussions of the K_S^0 FFs, we first, present the optimal set of K_S^0 FFs parameters which have been derived by minimizing the χ^2 as defined in Eq. (7) by comparing to the measured SIA data presented in Table I. The details of the fit are summarized in Table III which shows the best fit values of the free parameters based on Eq. (7).

We now discuss the overall statistical quality of the fit as measured by the total χ^2 per degree of freedom for the SAK20 K_S^0 fit. We find that the total $\chi^2/$d.o.f. of 1.161 and 1.124 for our NLO and NNLO QCD analysis, respectively, indicating a good quality of fit. Furthermore, as one can see from Table I, the inclusion of higher-order QCD correction leads to a smaller value for $\chi^2/$d.o.f. which indicates that our NNLO analysis improve the fit quality.

In the following, we now turn to discuss the K_S^0 FFs and their uncertainties obtained from the global fit. As we explained in more detail in Sec. IV, the present analyses adopt the most traditional fitting framework at NLO and NNLO accuracy assuming a very flexible functional form to parametrize the FFs at an initial scale. The SIA data analyzed in this study could not discriminate between quark and antiquark FFs. Hence, we display in Fig. 3 the

SAK20 results for $zD_i^{K_S^0}(z, Q)$, $i = d^+, u^+, s^+, c^+, b^+$ and g at the initial scale of $Q_0 = 5$ GeV. To investigate the effect of higher order correction, we prepare a comparison between NLO and NNLO fit results and their uncertainties in Fig. 3. Although there is no significant change in size for quarks and gluon FFs, a small difference between NLO and NNLO can be observe for $zD_{c^+}^{K_S^0}(z, Q)$ and $zD_g^{K_S^0}(z, Q)$. As we mentioned before, the uncertainty bands of FFs presented for the choice of tolerance $T = \Delta\chi^2 = 1$ for the 68% (one-sigma) confidence level (CL) obtained using Eq. (10). Figure 3 also shows that the errors for the gluon and u^+ FFs are large in both NLO and NNLO, which means that they are not well determined particularly at small value of Q.

In order to investigate the impact of the inclusion of higher order corrections in more details, in Fig. 4, we show the ratios of NNLO SAK20 FFs (magenta bands) to the corresponding NLO results (green bands) at $Q = M_Z$. As can be seen, the NLO and NNLO uncertainties presented in this figure are similar in size showing that the improvements of FFs uncertainty upon inclusion of higher-order QCD corrections are not significant when going from NLO to NNLO. However, the total $\chi^2/$d.o.f. that we obtained indicates that the inclusion of NNLO QCD corrections slightly improves the overall fit quality as well as the description of the data.

In Fig. 5, the obtained $zD_i^{K_S^0}(z, Q)$, $i = d^+, u^+, s^+, c^+, b^+$, and g from our analysis as function of z are presented at NNLO accuracy at $Q = M_Z$, and compared them with the results obtained by AKK08 FFs Collaboration [34].
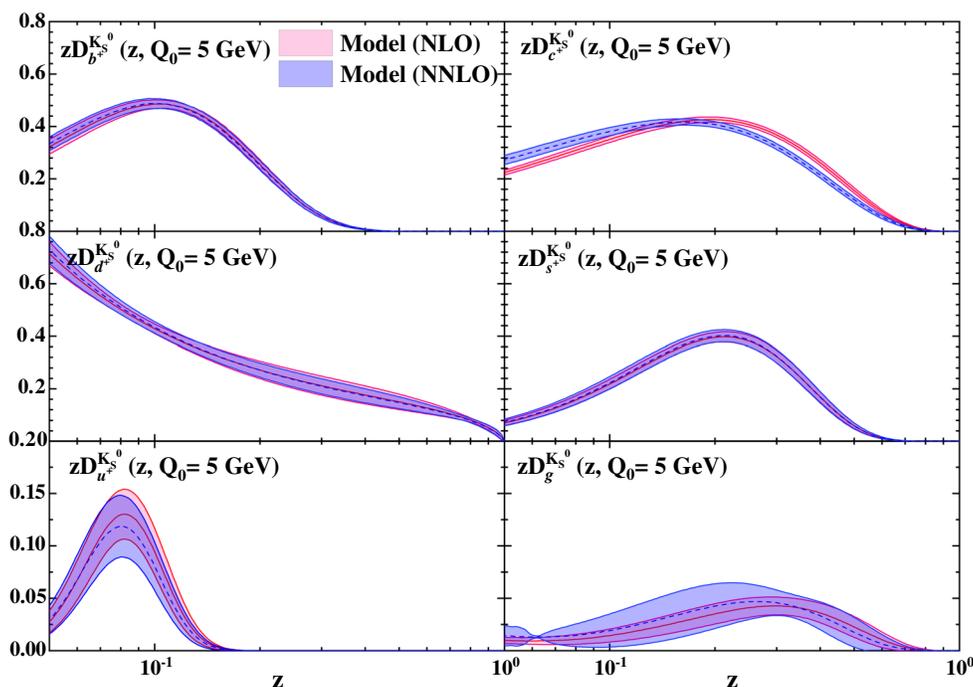
FIG. 3. The obtained $zD^{K_S^0}(z, Q)$ for all kinds of partons at NLO and NNLO accuracy, defined in Eq. (7), at our initial scale of $Q_0 = 5$ GeV. The shaded bands correspond to uncertainty estimates based on Eq. (10) for $\Delta\chi^2 = 1$.
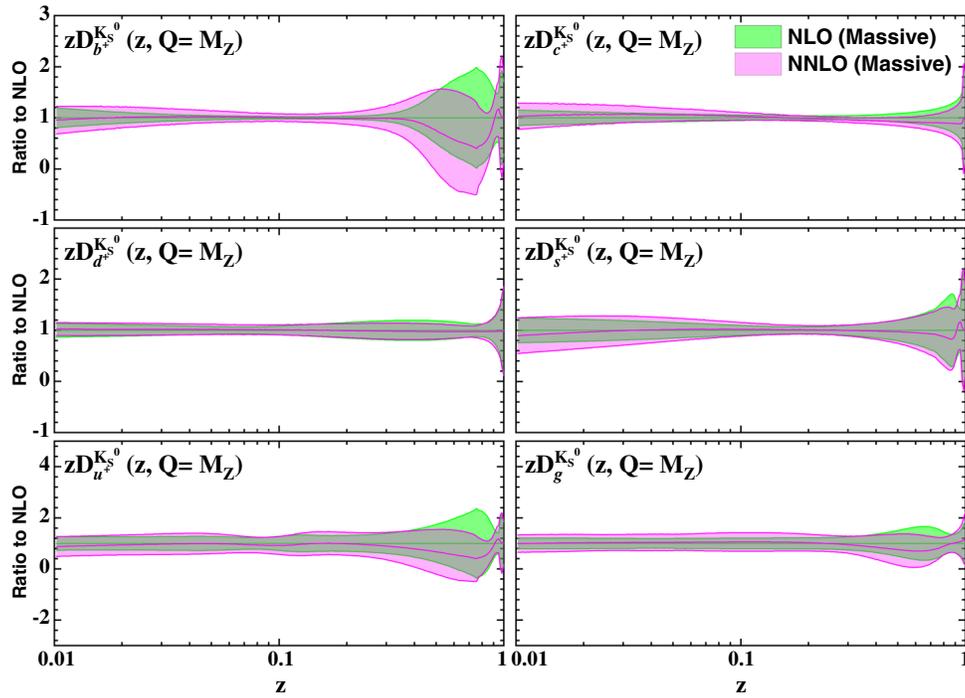
FIG. 4. The ratios of NNLO SAK20 FFs (magenta bands) to the corresponding NLO results (green bands). The shaded bands correspond to the uncertainty estimation based on Eq. (10) for $\Delta\chi^2 = 1$.

The shaded bands correspond to the uncertainty estimation based on Hessian approach for $\Delta\chi^2 = 1$. Concerning the shapes of the K_S^0 FFs, several interesting differences between SAK20 and AKK08 can be seen from the comparisons in Fig. 5. Compared to the AKK08 FFs, one can see weak agreements between two results except for the c^+ distribution. Fig. 5 shows that the SAK20 FFs for u^+, b^+ and gluon densities are smaller than AKK08 for the
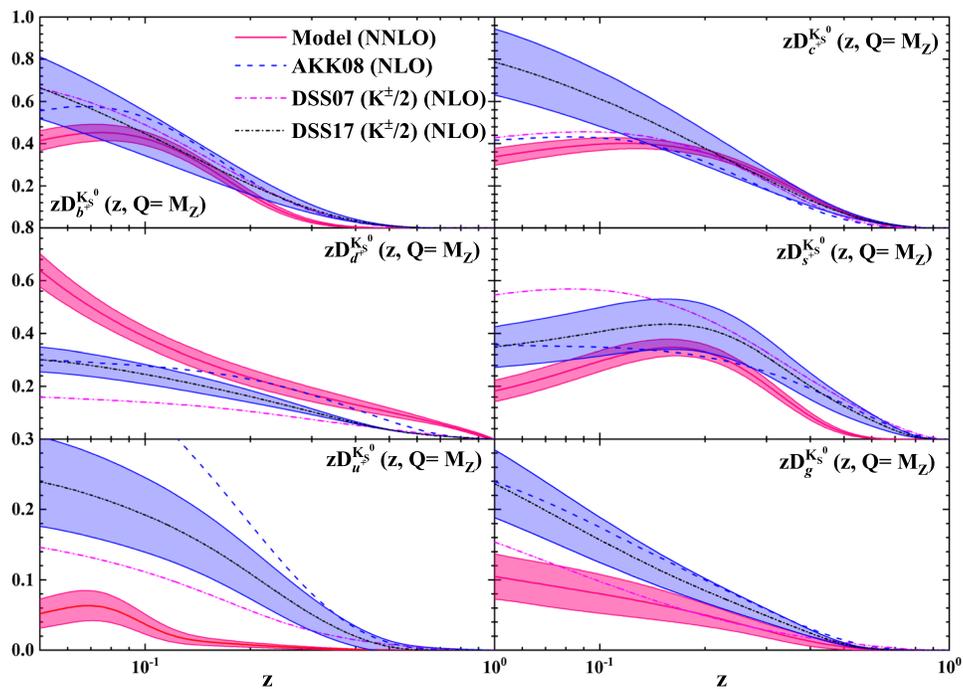
FIG. 5. The obtained $zD^{K_S^0}(z, Q)$ for all kinds of partons, at NNLO accuracy at $Q = M_Z$. The shaded bands correspond to the uncertainty estimates based on Eq. (10) for $\Delta\chi^2 = 1$. The corresponding results from AKK08 [34] for K_S^0 FFs and, DSS07 [8] and DSS17 [9] for $K^\pm/2$ at NLO also are shown for comparison.

medium to small value of z. For the case of d^+ FF, one can see that, the AKK08 is smaller than our result for the whole range of z. The origin of the differences among the SAK20 and AKK08 over the whole z range, is likely to be mostly due to the inclusion of inclusive hadron production measurements from proton-proton collisions data in AKK08 while SAK20 is limited to the SIA data only.

In the following, we compare our results for the K_S^0 FFs with those of $K^\pm$ FFs from DSS07 [8] and DSS17 [9]. These comparisons could be done using the approximation relation between K_S^0 FFs with those of $K^\pm$ FFs, i.e.,

$$D_i^{K_S^0} = \frac{1}{2} D_j^{K^\pm}$$

where $i = u$, d if $j = d$, u, otherwise $i = j$ [34]. In both DSS07 and DSS17 studies, a global QCD analysis has been done for parton-to-kaon FFs at NLO accuracy using the most recent experimental information for $K^\pm$ production in SIA process, lepton-nucleon (ℓ-N) DIS, and proton-proton (pp) collisions. As can be seen from Fig. 5, the most noticeable finding emerges from these comparisons is the good agreement for the case of charm-quark and gluon FFs between our results and DSS07. In other cases, one can see that these results are different in shape. However, for the case of bottom-quark FFs, DSS07 and DSS17 are in good agreement with each other. The origin of the difference between our results and DSS analyses is using the $K^\pm$ data sets in DSS and K^0 in our analysis.

A further noticeable aspect of the comparison presented in Fig. 5 is related to the size of the FF uncertainties. As one can see from this plot, while the SAK20 and DSS17 uncertainties for the case of gluon and d^+ FFs are similar in size, the uncertainty bands for other parton species are in general visibly different, particularly those of the u^+ and s^+ FFs. These differences are expected due to the different fit methodology, i.e., the Hessian method with a fixed input parameterizations in SAK20 case. As we mentioned, we employ the standard parameter-fitting criterion by considering the tolerance of $T = \Delta\chi^2_{\text{global}} = 1$ at the 68% (1-σ) confidence level (CL).

B. The results of $\Lambda/\bar{\Lambda}$ FFs and their uncertainties

In this section, first we mentioned the best fit values of $\Lambda/\bar{\Lambda}$ free parameters presented in Table IV which have been derived from QCD fit from SIA data. Then we consider the total χ^2/d.o.f. and they are equal to 1.601 and 1.602 at NLO and NNLO, respectively, and indeed we can not see the noticeable improvement in χ^2/d.o.f. value at NNLO in comparison to NLO accuracy.

In the following, we now turn to discuss our results and findings for the determination of $\Lambda/\bar{\Lambda}$ FFs and their uncertainties. In order to study the perturbative convergence of the $\Lambda/\bar{\Lambda}$ FFs upon inclusion of higher order QCD corrections, we first compare our NLO, and NNLO determinations among each other at the input scale. The same comparison will be presented as ratios of NNLO SAK20 FFs to the corresponding NLO results. Then, we compare our best-fit NNLO $\Lambda/\bar{\Lambda}$ FFs to their counterparts in the AKK analysis at the scale of M_Z.

In the following, we show the FFs results and their uncertainties at NLO and NNLO accuracy, focusing on their perturbative convergence upon inclusions of higher-order QCD corrections. We display the six FFs combinations parameterized in our QCD fits for the $\Lambda/\bar{\Lambda}$ hadrons, and their 1-σ uncertainties in Fig. 6. For each partonic species, the FFs are shown at NLO and NNLO as functions of z at our input scale $Q_0 = 5$ GeV. A noticeable aspect of the comparisons in Fig. 6 are related to the shape and the size of the FF uncertainties. The u^+, d^+, and b^+ FFs are similar in shape, while for other FFs, a small differences are observed. For both NLO and NNLO FFs, the s^+ and gluon FFs turn to zero for small values of $z < 0.2$. Overall, the differences between NLO and NNLO FFs are slightly small. This is consistent with the perturbative convergence of the global χ^2 that we discussed in Sec. II, (see the χ^2/d.o.f. presented in Table II).

In order to judge the effect arising from these corrections, we present in Fig. 7 the ratios of NNLO SAK20 FFs to the corresponding NLO results at the scale of $Q = M_Z$ as functions of z. While the b^+ and d^+ uncertainties are seem to be similar in size, the s^+, u^+ and gluon FFs uncertainty bands are in general smaller at NNLO accuracy, particularly those of the s^+ and u^+ FFs. The uncertainty band for the c^+ NNLO FFs is visibly larger at small value of z and smaller at large values for z. Although the total χ^2/d.o.f. presented in Table II indicate that there is no improvement from NLO to NNLO accuracy, the findings in this figure show the reduction of error bands for three partons at NNLO in comparison to the NLO.

We now compare SAK20 FFs to the recent determination available in the literature, namely the AKK08 [34] FFs set. Their analysis is performed only at NLO accuracy. Such a comparisons are shown in Fig. 8 at $Q = M_Z$ for all partonic species. Concerning the shapes of these FFs, several interesting differences between these two sets can be seen from the comparisons in Fig. 8. As can be seen, for the b^+ FFs, the SAK20 and AKK08 results are in good agreement. For other parton species, the differences in shape among these two FF sets are more marked than in the case of b^+ FFs and relatively large differences are observed. The origin of differences among these two FF sets, at small to medium values of z for most of the quark FFs and the gluon FF, is likely to be mostly due to the inclusive hadron production measurements from proton-proton reactions that AKK08 included in their analysis but it is not considered in the SAK20 FFs sets.
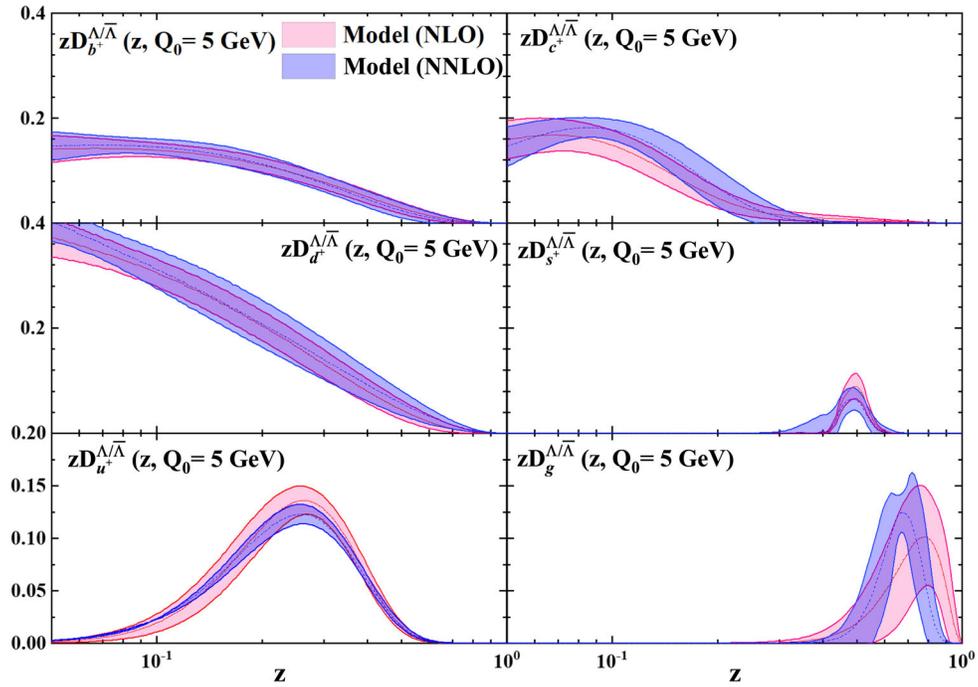
FIG. 6.   Same as Fig. 3 but for $\Lambda/\bar{\Lambda}$.

VII. FIT QUALITY AND COMPARISON TO THE SIA DATA

This section deals with our global fit results in term of fit quality and detailed comparison to the SIA experimental measurements. First, we compare our NNLO theory predictions with the K_S^0 production data analyzed in this study. Then, we present the comparison of our theory predictions with the $\Lambda/\bar{\Lambda}$ production cross section measurements. In Tables I and II, we report the χ^2 per point for each datasets and total χ^2 per degree of freedom included in the SAK20 FFs analysis. The values are shown at NLO and NNLO accuracy for both K_S^0 and $\Lambda/\bar{\Lambda}$ FFs determinations.
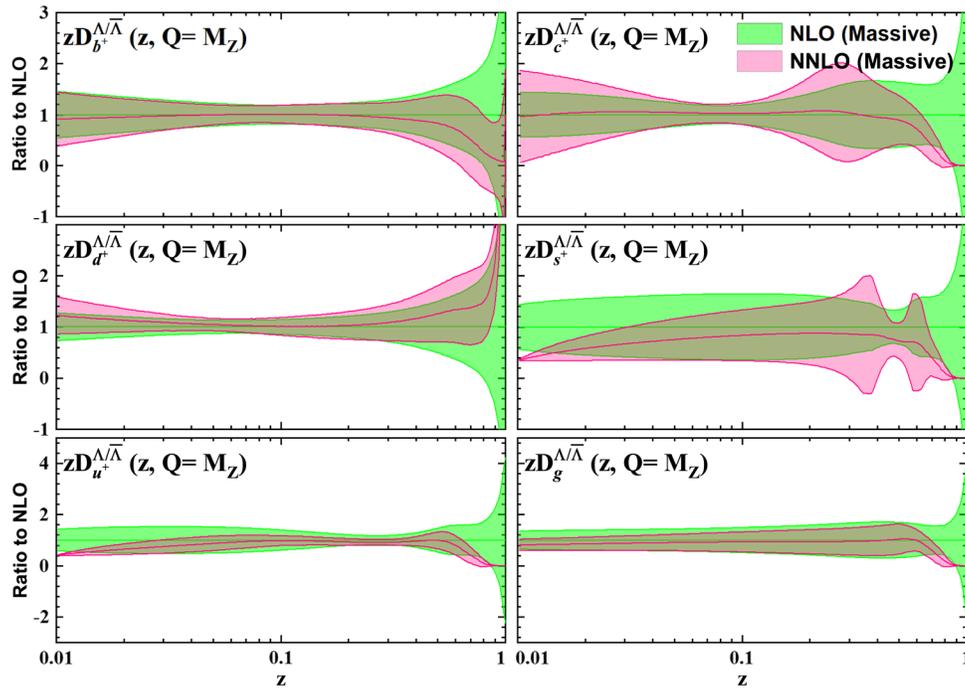
FIG. 7.   Same as Fig. 4 but for $\Lambda/\bar{\Lambda}$.
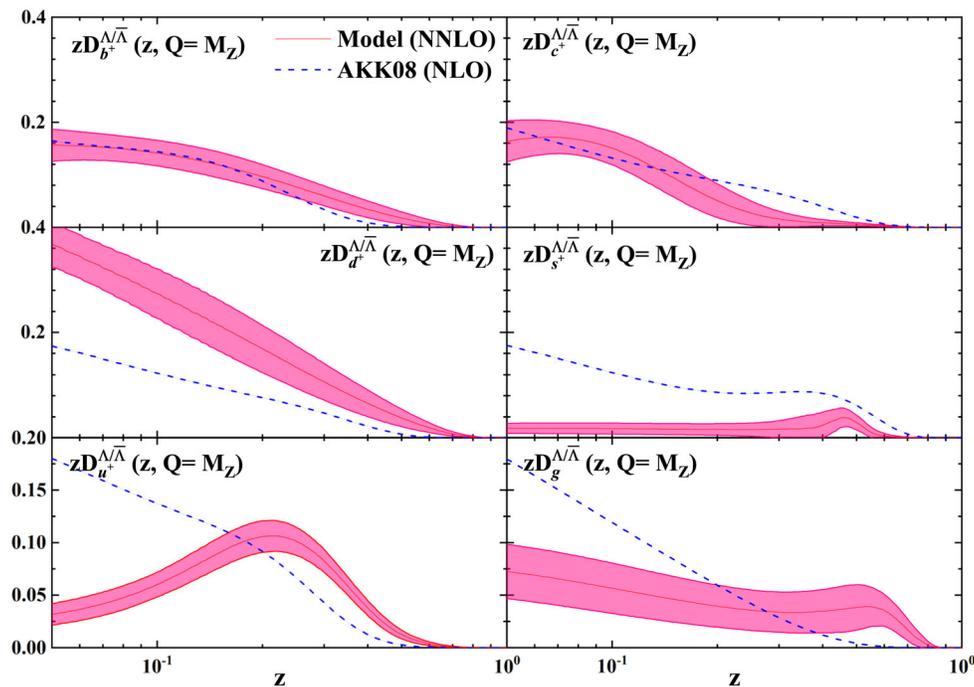
FIG. 8. Same as Fig. 5 but for $\Lambda/\bar{\Lambda}$.

Concerning the fit quality of the total SIA datasets analyzed in SAK20, the most noticeable feature is that the $\chi^2/$d.o.f. value for K_S^0 shows almost 3% improvement on total χ^2 when the higher order correction is considered. However, for the case of $\Lambda/\bar{\Lambda}$ the values of $\chi^2/$d.o.f. are almost the same at NLO and NNLO accuracy.

Comparison between the K_S^0 production dataset in SIA process analyzed in this study from different experiments and the corresponding theoretical predictions using SAK20 best-fit at NNLO accuracy are shown in Figs. 9–11. We show the comparisons as the data/theory ratios. The error bands indicate to the 1-σ FF uncertainties. In Fig. 9, comparisons are displayed for the TASSO data for different center-of-mass energies. In Fig. 10, we show the same comparison for all the inclusive experimental data analyzed in this study, except the SLD. Deviation between the theory and the data can be seen for the large value of z for HRS, DELPHI 183 and DELPHI 189. These findings consistent with the χ^2 values listed in Table I. The data/theory ratios for the SLD measurements in inclusive, uds-, c-, b- tagged are presented in Fig. 11. One can see a good agreement between SLD inclusive, uds- and b- tagged data and theory predictions at NNLO accuracy obtained from our QCD fit. However, the agreement between SLD c- tagged data and our theory is not as well as the others SLD data.

In Fig. 12, the comparisons have been shown between the theoretical predictions using SAK20 and the TASSO $\Lambda/\bar{\Lambda}$ production for different center of mass energy. According to Fig. 12 and Table II, the TASSO 34.8 dataset is in good agreement in low and medium z regains

with theoretical prediction obtain from our QCD analysis. This plot also reveals that our theoretical prediction could not describe the latest data point in large z region. Comparison between the $\Lambda/\bar{\Lambda}$ production and our results is shown in Fig. 13 for all the inclusive experimental data except SLD. Finally, a comparison with the SLD data in inclusive, uds-, c-, b- tagged for $\Lambda/\bar{\Lambda}$ production are shown in Fig. 14. In general, an overall good agreements between the data from all experiments and SAK20 NNLO theoretical predictions are achieved, which consistent with the individual χ^2 values reported in Tables I and II. Remarkably, our theoretical predictions and the data are in good agreements from small to and large values of z.

VIII. IMPACT OF HADRON MASS CORRECTIONS

In order to study the effects arising from the hadron mass corrections, we perform the analyses in which we do not consider hadron mass corrections for K_S^0 and $\Lambda/\bar{\Lambda}$ and repeat our QCD fits just at NNLO accuracy. We entitle this analysis to *massless* and our main analyses by considering hadron mass corrections is called *massive*. Finally, in order to investigate in details the effects arising from the inclusion of such corrections on our K_S^0 and $\Lambda/\bar{\Lambda}$ FFs determinations, we compare the results of our *massless* and *massive* analyses. It is worth mentioning here that such corrections could affect the small z regions [1].

In Fig. 15 we show the comparison between our *massless* and *massive* results as ratio, to investigate the effects of mass
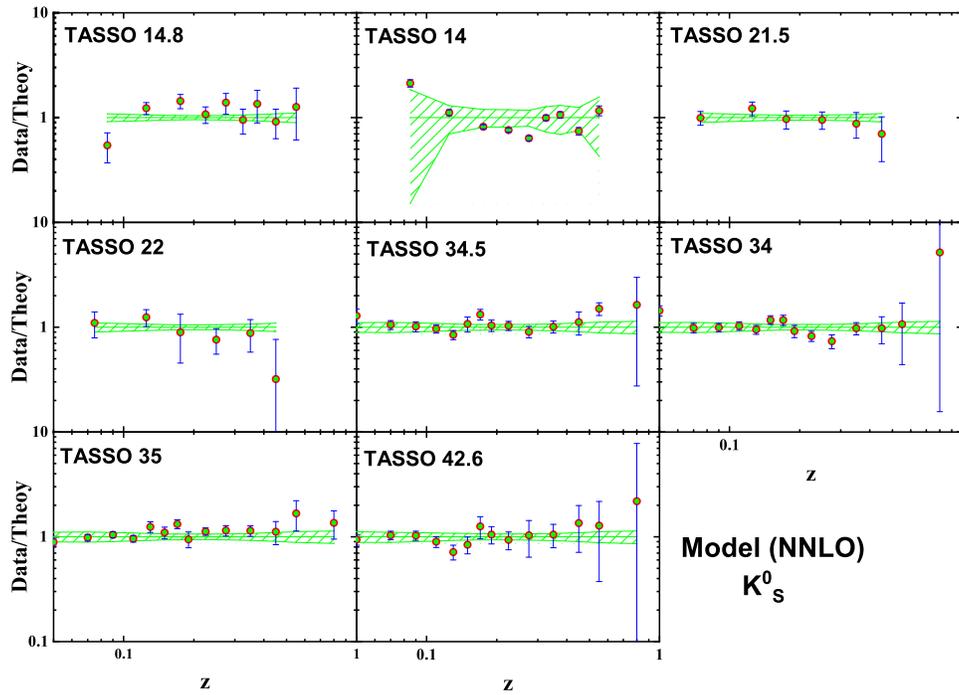
FIG. 9. Comparison between the K_S^0 production cross section analyzed in this study from different experiments by TASSO Collaboration [41,42]. The comparisons have been shown as data/theory ratios. The error bands indicate to the one-σ FF uncertainties. The results shown in this plots are correspond to SAK20 NNLO fit in the presence of hadron-mass corrections.

correction for all parton species as function of z at $Q = M_Z$. As can be seen, the central values of d^+, s^+ and c^+ are not affected noticeably by considering mass corrections, the central values for u^+, b^+ and g change remarkably in medium to large z regions. There are differences for the error bands between two analyses, specifically at small values of z. The reduction of uncertainties in the region $z < 0.1$ can be seen for all partons in *massive* analysis. However, the
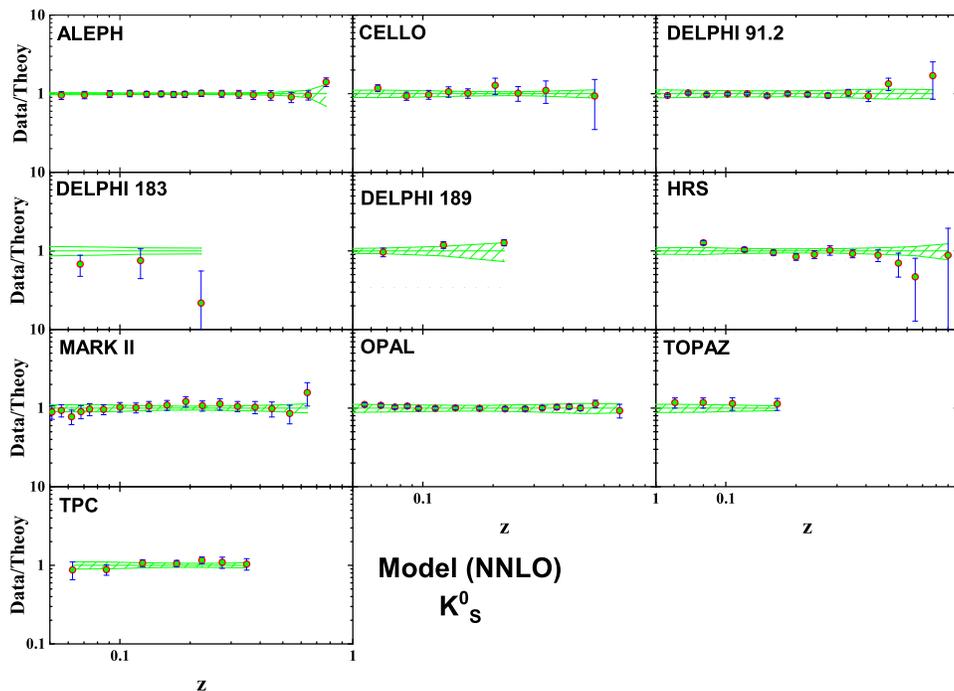
FIG. 10. Same as Fig. 9 but for the SIA data from HRS [43], TPC [44], MARK II [45], CELLO [46], TOPAZ [47], ALEPH [48], DELPHI [49,51], OPAL [37] and SLD [50] Collaborations.
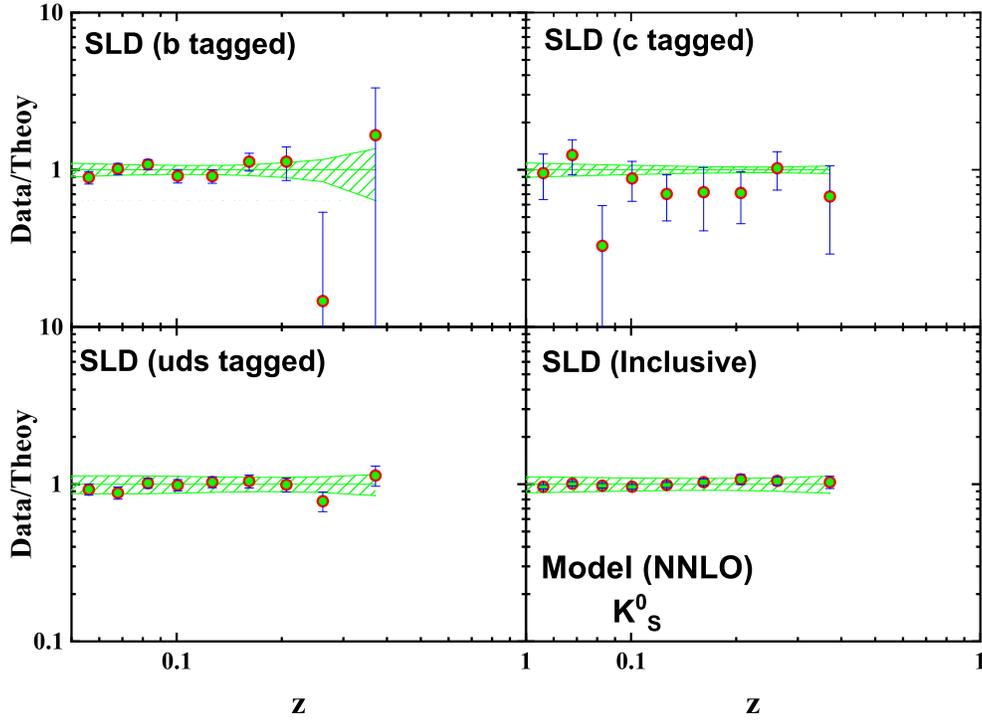
FIG. 11.   Same as Fig. 9 but for inclusive, *uds*-, *c*- and *b*-tagged data from SLD [50] Collaboration.

error bands increase for the $z > 0.1$ in *massive* analysis for all the partons, except c^+. Also the rise of error uncertainties for u^+ and b^+ are dramatic. According to Fig. 1, statistically the K_S^0 experimental data included in our analysis for

$z < 0.6$ is more than for $z > 0.6$. Consequently, more data points at large values of z could constrain the FFs.

We are now in a position to compare the SAK20 FFs for $\Lambda/\bar{\Lambda}$ with and without the hadron mass effects at NNLO
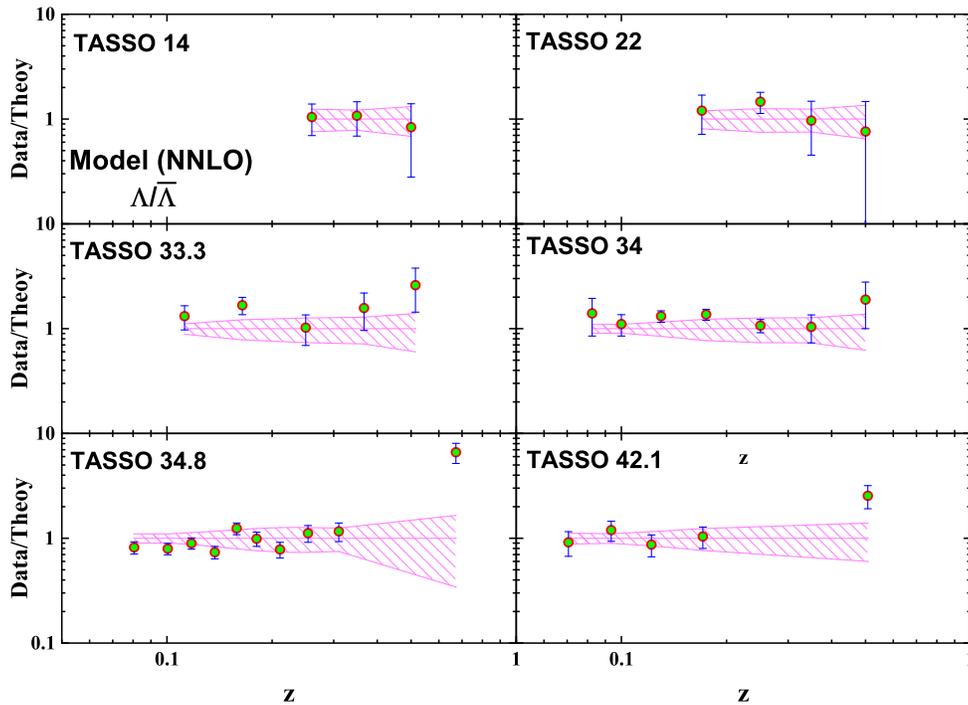
FIG. 12.   Same as Fig. 9 but this time the comparisons have been shown between the theoretical predictions using SAK20 and the corresponding $\Lambda/\bar{\Lambda}$ production datasets from different experiments of *TASSO* Collaboration [41,42].
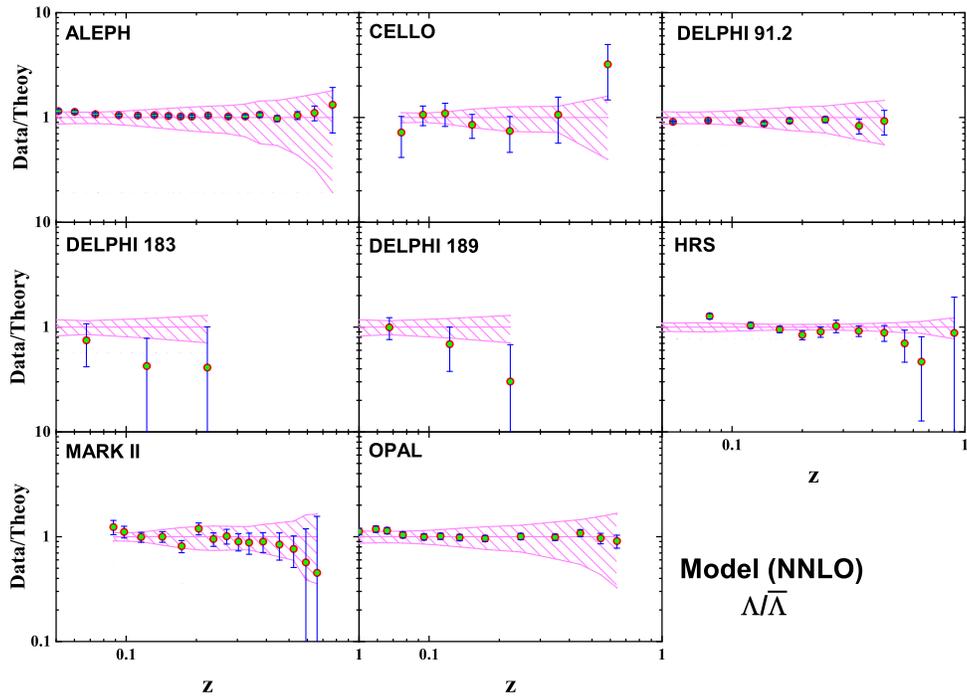
FIG. 13.   Same as Fig. 12 but for HRS [43], MARK II [45], CELLO [46], ALEPH [48], DELPHI [49,51] and OPAL [37] Collaborations datasets.

accuracy. Such comparisons are shown in Fig. 16 as a ratios to the SAK20 FFs without such corrections. Concerning the FF uncertainties upon inclusion of hadron mass corrections, we observe that for the quark and gluon distributions,

including such corrections significantly affect the uncertainty bands. The smaller uncertainties of the SAK20 FFs in the presence of hadron mass effects as shown in Fig. 16 may be due the fact that such corrections affect the shape
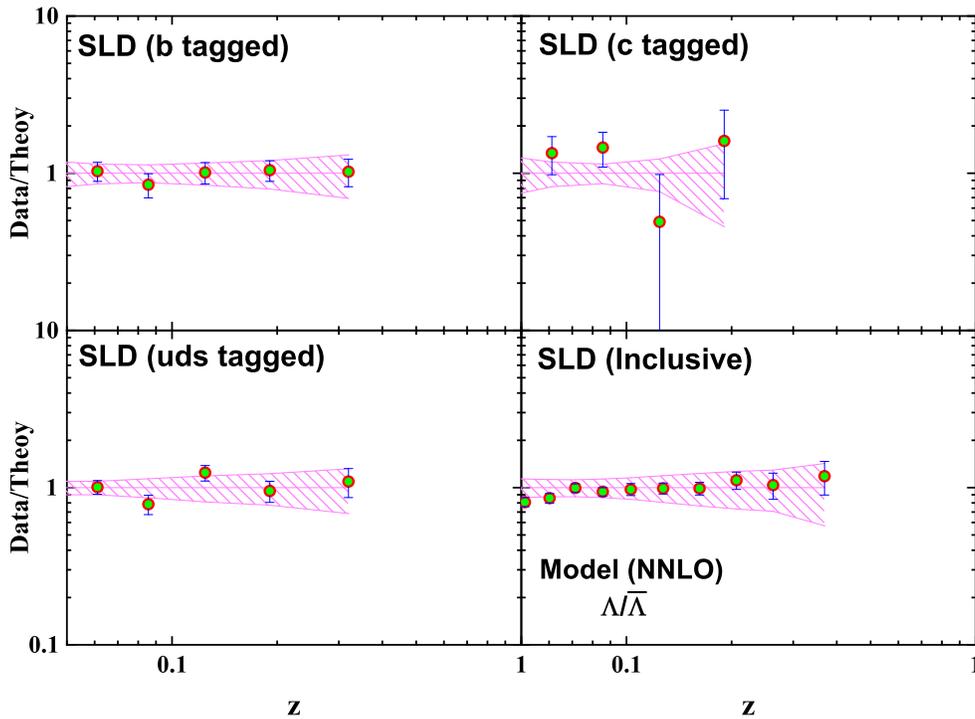
FIG. 14.   Same as Fig. 12 but for SLD [50] Collaboration datasets in inclusive, *uds*-, *c*- and *b*- tagged.
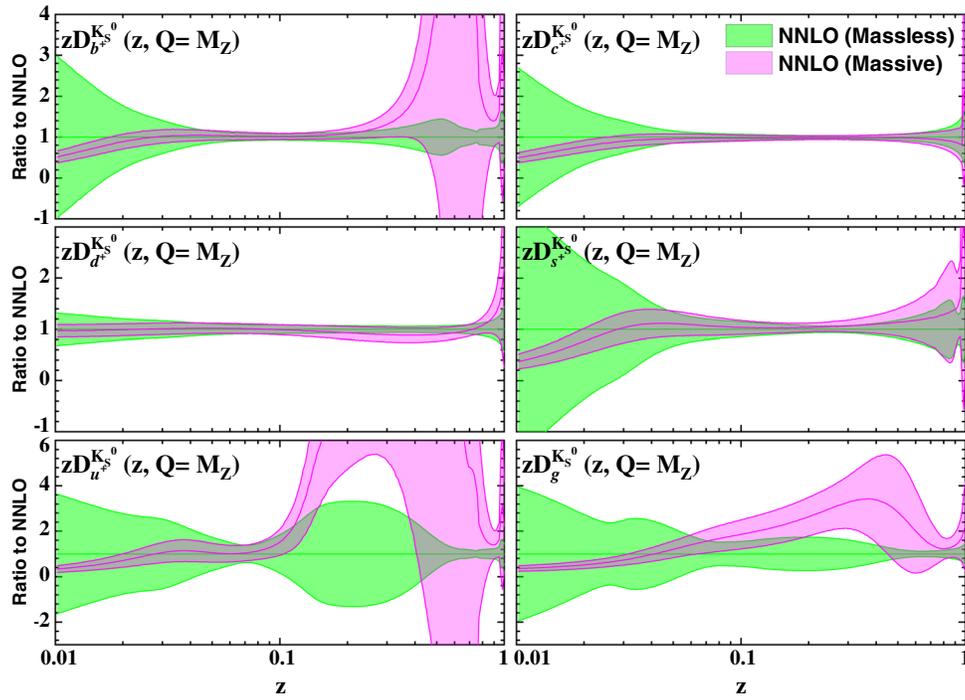
FIG. 15. The ratios of massive NNLO SAK20 FFs to the corresponding massless NNLO results. The shaded bands correspond to uncertainty estimates based on Eq. (10) for $\Delta\chi^2 = 1$.

and the uncertainty bands at small values of z. As can be seen from Fig. 16, the hadron mass corrections significantly affect the central values of d^+, s^+, c^+, and b^+ more than u^+ and g FFs. The hadron mass corrections decrease the uncertainties for u^+ and g in all range of z, and for s^+

in the range of $z < 0.3$. The behavior of error bands treat differently for d^+, c^+, and b^+ for whole range of z.

As a conclusion, applying the hadron mass corrections in our analyses for K_S^0 and $\Lambda/\bar{\Lambda}$ can generally decrease the error bands of FFs in small z region. As expected from
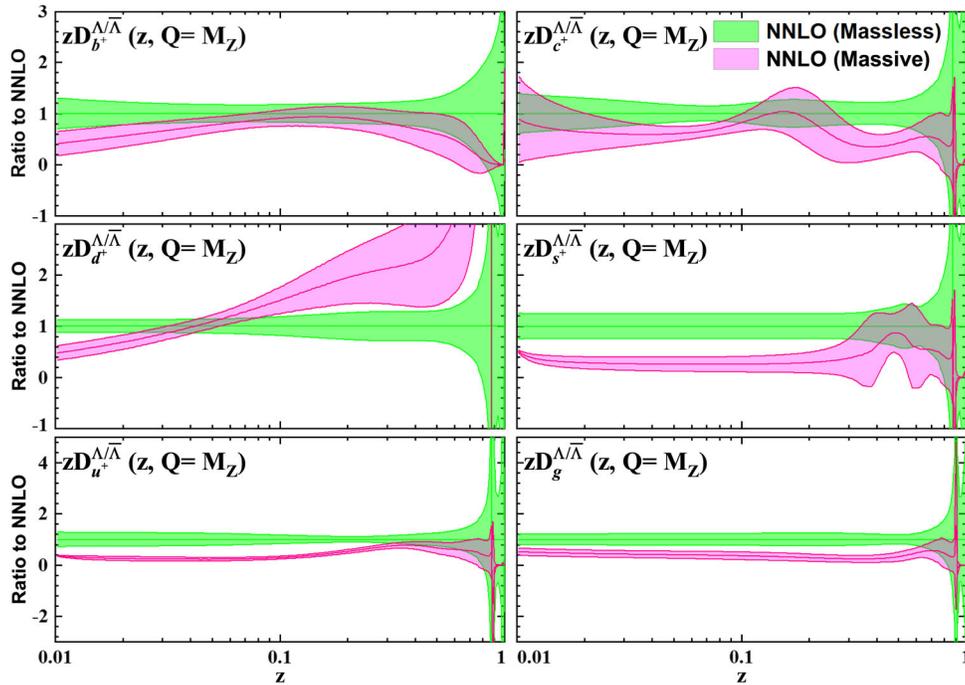
FIG. 16. Same as Fig. 15 but for $\Lambda/\bar{\Lambda}$.

Eq. (6) including the hadron mass corrections strongly depend on the hadron mass m_h, and hence, the kind of hadron. Then this corrections affected the $\Lambda/\bar{\Lambda}$ more than K_S^0, see Figs. 15 and 16. According to Figs. 1 and 2 the number of data from SIA process for K_S^0 and $\Lambda/\bar{\Lambda}$ production are being poor at $z > 0.6$. Hence, one can see the large uncertainties in this region.

IX. SUMMARY AND CONCLUSIONS

As a summary, the main goal of the current study is to present the new sets of FFs for K_S^0 and $\Lambda/\bar{\Lambda}$ from QCD analyses of single-inclusive electron-positron annihilation process (SIA) at NLO, and for the first time, at NNLO accuracy in pQCD. These analyses are based on comprehensive experimental datasets in which include the precise measurements of K_S^0 and $\Lambda/\bar{\Lambda}$ production cross sections in the SIA process. Well-established QCD fitting methodology used to determine K_S^0 and $\Lambda/\bar{\Lambda}$ FFs.

In this analysis, we have introduced several methodological improvements to determined the FFs. As a first improvement, we have performed the first QCD analysis at NNLO approximation to clarify the role of the higher-order QCD corrections on the description of the data. The related results are clearly presented in this paper and compared to our NLO study and the corresponding results from AKK08 [34]. As a next improvement, the calculations of these new FFs for K_S^0 and $\Lambda/\bar{\Lambda}$ are along with the determination of uncertainties. The 'Hessian' method is used to provide a

faithful representation of the experimental uncertainties. In addition, we apply the K_S^0 and $\Lambda/\bar{\Lambda}$ mass corrections in our analyses to include the low-z data points. We also study the hadron mass effects on the different species of patrons and their error bands. As a final point, the analysis reported in this paper represents the first step of a broader project, and hence, a number of improvements are foreseen. SAK20 analyses are based only on the SIA measurements for the K_S^0 and $\Lambda/\bar{\Lambda}$ production measurements. Although the SIA data is the cleanest process for FFs determination, it may not possible to consider the flavor separation. It is also a little sensitive to the gluon FF. Hence, the FFs presented in this paper could be improved by adding the data from proton-proton (pp) collisions in our data sample. Gluon FFs could be well-constrained by the hadron collider data. A further improvement would be the inclusion of heavy-quark mass corrections in which could improve the description of the data, especially at the lowest center-of-mass energy. The SAK20 FFs for the K_S^0 and $\Lambda/\bar{\Lambda}$ presented in this work are available via the standard LHAPDF interface [69].

ACKNOWLEDGMENTS

---

[1] V. Bertone, S. Carrazza, N. P. Hartland, E. R. Nocera, and J. Rojo (NNPDF Collaboration), A determination of the fragmentation functions of pions, kaons, and protons with faithful uncertainties, Eur. Phys. J. C **77**, 516 (2017).

[2] J. J. Ethier, N. Sato, and W. Melnitchouk, First Simultaneous Extraction of Spin-Dependent Parton Distributions and Fragmentation Functions from a Global QCD Analysis, Phys. Rev. Lett. **119**, 132001 (2017).

[3] V. Bertone, N. P. Hartland, E. R. Nocera, J. Rojo, and L. Rottoli (NNPDF Collaboration), Charged hadron fragmentation functions from collider data, Eur. Phys. J. C **78**, 651 (2018).

[4] M. Soleymaninia, M. Goharipour, and H. Khanpour, First QCD analysis of charged hadron fragmentation functions and their uncertainties at next-to-next-to-leading order, Phys. Rev. D **98**, 074002 (2018).

[5] M. Salajegheh, S. M. M. Nejad, M. Soleymaninia, H. Khanpour, and S. A. Tehrani, NNLO charmed-meson fragmentation functions and their uncertainties in the presence of meson mass corrections, Eur. Phys. J. C **79**, 999 (2019).

[6] M. Salajegheh, S. M. M. Nejad, H. Khanpour, B. A. Kniehl, and M. Soleymaninia, B-hadron fragmentation functions at next-to-next-to-leading order from a global analysis of e^+e^- annihilation data, Phys. Rev. D **99**, 114001 (2019).

[7] M. Epele, C. G. Canal, and R. Sassot, Heavy quark mass effects in parton-to-kaon hadronization probabilities, Phys. Lett. B **790**, 102 (2019).

[8] D. de Florian, R. Sassot, and M. Stratmann, Global analysis of fragmentation functions for pions and kaons and their uncertainties, Phys. Rev. D **75**, 114010 (2007).

[9] D. de Florian, M. Epele, R. J. Hernandez-Pinto, R. Sassot, and M. Stratmann, Parton-to-kaon fragmentation revisited, Phys. Rev. D **95**, 094019 (2017).

[10] G. R. Boroun, S. Zarrin, and S. Dadfar, Laplace method for the evolution of the fragmentation function of B_c mesons, Nucl. Phys. **A953**, 21 (2016).

[11] M. Soleymaninia, M. Goharipour, H. Khanpour, and H. Spiesberger, Simultaneous extraction of fragmentation functions of light charged hadrons with mass corrections, arXiv:2008.05342.

[12] M. Delpasand, S. M. M. Nejad, and M. Soleymaninia, Λ_c^+ fragmentation functions from pQCD approach and the Suzuki model, Phys. Rev. D **101**, 114022 (2020).

[13] M. Soleymaninia and H. Khanpour, Transverse momentum dependent of charged pion, kaon, and proton/antiproton fragmentation functions from e^+e^- annihilation process, Phys. Rev. D **100**, 094033 (2019).

[14] Z. B. Kang, A. Prokudin, P. Sun, and F. Yuan, Extraction of quark transversity distribution and collins fragmentation functions with QCD evolution, Phys. Rev. D **93**, 014009 (2016).

[15] M. Boglione, J. O. Gonzalez-Hernandez, and R. Taghavi, Transverse parton momenta in single inclusive hadron production in e^+e^- annihilation processes, Phys. Lett. B **772**, 78 (2017).

[16] M. Anselmino, M. Boglione, U. D'Alesio, F. Murgia, and A. Prokudin, Role of transverse momentum dependence of unpolarized parton distribution and fragmentation functions in the analysis of azimuthal spin asymmetries, Phys. Rev. D **98**, 094023 (2018).

[17] R. Seidl et al. (Belle Collaboration), Transverse momentum dependent production cross sections of charged pions, kaons and protons produced in inclusive e^+e^- annihilation at $\sqrt{s} = 10.58$ GeV, Phys. Rev. D **99**, 112006 (2019).

[18] J. C. Collins, D. E. Soper, and G. F. Sterman, Factorization of hard processes in QCD, Adv. Ser. Dir. High Energy Phys. **5**, 1 (1989).

[19] G. Kramer and H. Spiesberger, Study of heavy meson production in p–Pb collisions at $\sqrt{S} = 5.02$ TeV in the general-mass variable-flavour-number scheme, Nucl. Phys. **B925**, 415 (2017).

[20] M. Benzke, B. A. Kniehl, G. Kramer, I. Schienbein, and H. Spiesberger, B-meson production in the general-mass variable-flavour-number scheme and LHC data, Eur. Phys. J. C **79**, 814 (2019).

[21] G. Kramer and H. Spiesberger, b-hadron production in the general-mass variable-flavour-number scheme and LHC data, Phys. Rev. D **98**, 114010 (2018).

[22] S. Chatrchyan et al. (CMS Collaboration), Study of high-pT charged particle suppression in PbPb compared to pp collisions at $\sqrt{s_{NN}} = 2.76$ TeV, Eur. Phys. J. C **72**, 1945 (2012).

[23] R. Sassot, M. Stratmann, and P. Zurita, Fragmentations functions in nuclear media, Phys. Rev. D **81**, 054001 (2010).

[24] B. A. Kniehl, G. Kramer, I. Schienbein, and H. Spiesberger, $\Lambda_c^\pm$ production in pp collisions with a new fragmentation function, Phys. Rev. D **101**, 114021 (2020).

[25] J. Adams et al. (STAR Collaboration), Identified hadron spectra at large transverse momentum in p + p and d + Au collisions at s(NN)**(1/2) = 200-GeV, Phys. Lett. B **637**, 161 (2006).

[26] I. Arsene et al. (BRAHMS Collaboration), Production of Mesons and Baryons at High Rapidity and High P(T) in Proton-Proton Collisions at s**(1/2) = 200- GeV, Phys. Rev. Lett. **98**, 252001 (2007).

[27] P. Azzi et al., Report from Working Group 1: Standard model physics at the HL-LHC and HE-LHC, CERN Yellow Rep. Monogr. **7**, 1 (2019).

[28] A. Dainese, M. Mangano, A. B. Meyer, A. Nisati, G. Salam, and M. A. Vesterinen, Report on the physics at the HL-LHC, and perspectives for the HE-LHC, 10.23731/CYRM-2019-007.

[29] A. Abada et al. (FCC Collaboration), FCC physics opportunities: Future circular collider conceptual design report volume 1, Eur. Phys. J. C **79**, 474 (2019).

[30] M. Salajegheh, S. M. M. Nejad, and M. Delpasand, Determination of D_s^+ meson fragmentation functions through two different approaches, Phys. Rev. D **100**, 114031 (2019).

[31] J. Binnewies, B. A. Kniehl, and G. Kramer, Neutral kaon production in e^+e^-, ep and $p\bar{p}$ collisions at next-to-leading order, Phys. Rev. D **53**, 3573 (1996).

[32] C. Bourrely and J. Soffer, Statistical approach for unpolarized fragmentation functions for the octet baryons, Phys. Rev. D **68**, 014003 (2003).

[33] S. Albino, B. A. Kniehl, and G. Kramer, Fragmentation functions for K0(S) and Lambda with complete quark flavor separation, Nucl. Phys. **B734**, 50 (2006).

[34] S. Albino, B. A. Kniehl, and G. Kramer, AKK update: Improvements from new theoretical input and experimental data, Nucl. Phys. **B803**, 42 (2008).

[35] M. Arneodo et al. (European Muon Collaboration), Measurements of the u valence quark distribution function in the proton and u quark fragmentation functions, Nucl. Phys. **B321**, 541 (1989).

[36] S. Belostotsky et al. (HERMES Collaboration), Study of Lambda hyperon production in the HERMES experiment, Acta Phys. Pol. B **33**, 3785 (2002).

[37] G. Abbiendi et al. (OPAL Collaboration), Leading particle production in light flavor jets, Eur. Phys. J. C **16**, 407 (2000).

[38] S. Albino, The hadronization of partons, Rev. Mod. Phys. **82**, 2489 (2010).

[39] J. Pumplin, D. Stump, R. Brock, D. Casey, J. Huston, J. Kalk, H. L. Lai, and W. K. Tung, Uncertainties of predictions from parton distribution functions. 2. The Hessian method, Phys. Rev. D **65**, 014013 (2001).

[40] A. D. Martin, W. J. Stirling, R. S. Thorne, and G. Watt, Parton distributions for the LHC, Eur. Phys. J. C **63**, 189 (2009).

[41] M. Althoff et al. (TASSO Collaboration), A detailed study of strange particle production in e^+e^- annihilation at high-energy, Z. Phys. C **27**, 27 (1985).

[42] W. Braunschweig et al. (TASSO Collaboration), Strange meson production in e^+e^- annihilation, Z. Phys. C **47**, 167 (1990).

[43] M. Derrick et al., Hadron production in e^+e^- annihilation at $\sqrt{s} = 29$-GeV, Phys. Rev. D **35**, 2639 (1987).

[44] H. Aihara et al. (TPC/Two Gamma Collaboration), K^{*0} and K_s^0 Meson Production in e^+e^- Annihilations at 29-GeV, Phys. Rev. Lett. **53**, 2378 (1984).

[45] H. Schellman et al., Measurement of $K^\pm$ and K^0 inclusive rates in e^+e^- annihilation at 29-GeV, Phys. Rev. D **31**, 3013 (1985).

[46] H. J. Behrend et al. (CELLO Collaboration), Inclusive strange particle production in e^+e^- annihilation, Z. Phys. C **46**, 397 (1990).

[47] R. Itoh et al. (TOPAZ Collaboration), Measurement of inclusive particle spectra and test of MLLA prediction in e^+e^- annihilation at s**(1/2) = 58-GeV, Phys. Lett. B **345**, 335 (1995).

[48] R. Barate *et al.* (ALEPH Collaboration), Studies of quantum chromodynamics with the ALEPH detector, Phys. Rep. **294,** 1 (1998).

[49] P. Abreu *et al.* (DELPHI Collaboration), Production characteristics of K0 and light meson resonances in hadronic decays of the Z0, Z. Phys. C **65,** 587 (1995).

[50] K. Abe *et al.* (SLD Collaboration), Production of pi+, K+, K0, K*0, phi, p and Lambda0 in hadronic Z0 decays, Phys. Rev. D **59,** 052001 (1999).

[51] P. Abreu *et al.* (DELPHI Collaboration), Charged and identified particles in the hadronic decay of W bosons and in e+e-—>q anti-q from 130-GeV to 200-GeV, Eur. Phys. J. C **18,** 203 (2000); Erratum, Eur. Phys. J. C **25,** 493 (2002).

[52] V. Bertone, S. Carrazza, and J. Rojo, APFEL: A PDF evolution library with QED corrections, Comput. Phys. Commun. **185,** 1647 (2014).

[53] A. Mitov and S. O. Moch, QCD corrections to semi-inclusive hadron production in electron-positron annihilation at two loops, Nucl. Phys. **B751,** 18 (2006).

[54] A. Mitov, S. Moch, and A. Vogt, Next-to-next-to-leading order evolution of non-singlet fragmentation functions, Phys. Lett. B **638,** 61 (2006).

[55] P. J. Rijken and W. L. van Neerven, Higher order QCD corrections to the transverse and longitudinal fragmentation functions in electron-positron annihilation, Nucl. Phys. **B487,** 233 (1997).

[56] V. N. Gribov and L. N. Lipatov, Deep inelastic e p scattering in perturbation theory, Yad. Fiz. **15,** 781 (1972) [Sov. J. Nucl. Phys. **15,** 438 (1972)].

[57] L. N. Lipatov, The parton model and perturbation theory, Yad. Fiz. **20,** 181 (1974) [Sov. J. Nucl. Phys. **20,** 94 (1975)].

[58] G. Altarelli and G. Parisi, Asymptotic freedom in parton language, Nucl. Phys. **B126,** 298 (1977).

[59] Y. L. Dokshitzer, Calculation of the structure functions for deep inelastic scattering and e^+e^- annihilation by perturbation theory in quantum chromodynamics, Zh. Eksp. Teor. Fiz. **73,** 1216 (1977) [Sov. Phys. JETP **46,** 641 (1977)].

[60] A. A. Almasy, S. Moch, and A. Vogt, On the next-to-next-to-leading order evolution of flavour-singlet fragmentation functions, Nucl. Phys. **B854,** 133 (2012).

[61] S. Moch and A. Vogt, On third-order timelike splitting functions and top-mediated Higgs decay into hadrons, Phys. Lett. B **659,** 290 (2008).

[62] T. Kneesch, B. A. Kniehl, G. Kramer, and I. Schienbein, Charmed-meson fragmentation functions with finite-mass corrections, Nucl. Phys. **B799,** 34 (2008).

[63] S. M. M. Nejad, M. Soleymaninia, and A. Maktoubian, Proton fragmentation functions considering finite-mass corrections, Eur. Phys. J. A **52,** 316 (2016).

[64] M. Tanabashi *et al.* (Particle Data Group), Review of particle physics, Phys. Rev. D **98,** 030001 (2018).

[65] R. D. Ball, S. Carrazza, L. Del Debbio, S. Forte, Z. Kassabov, J. Rojo, E. Slade, and M. Ubiali (NNPDF Collaboration), Precision determination of the strong coupling constant within a global PDF analysis, Eur. Phys. J. C **78,** 408 (2018).

[66] D. de Florian, R. Sassot, M. Epele, R. J. Hernández-Pinto, and M. Stratmann, Parton-to-pion fragmentation reloaded, Phys. Rev. D **91,** 014035 (2015).

[67] M. Soleymaninia, M. Goharipour, and H. Khanpour, Impact of unidentified light charged hadron data on the determination of pion fragmentation functions, Phys. Rev. D **99,** 034024 (2019).

[68] F. James and M. Roos, Minuit: A system for function minimization and analysis of the parameter errors and correlations, Comput. Phys. Commun. **10,** 343 (1975); F. James, MINUIT function minimization and error analysis: Reference manual version 94.1, CERN-D-506, CERN-D506.

[69] A. Buckley, J. Ferrando, S. Lloyd, K. Nordström, B. Page, M. Rüfenacht, M. Schönherr, and G. Watt, LHAPDF6: Parton density access in the LHC precision era, Eur. Phys. J. C **75,** 132 (2015).